

Effect of Exfoliated Graphene on Thermal Conductivity Enhancements of Graphene-Ironoxide Hybrid Nanofluids: Experimental Investigation and Effective Medium Theories

A. Arifutzzaman^{1,4,a*}, Ahmad Faris bin Ismail^{2,b}, Md Zahangir Alam^{3,c}, Ahsan Ali Khan^{4,d} and Saidur Rahman^{1,5,e}

¹Research Centre for Nanomaterials and Energy Technology (RCNMET), School of Science and Technology, Sunway University, No. 5, Jalan Universiti, Bandar Sunway, Petaling Jaya, 47500 Selangor Darul Ehsan, Malaysia.

²Department of Mechanical Engineering, Faculty of Engineering, International Islamic University Malaysia, Malaysia

³Department of Biotechnology Engineering, Faculty of Engineering, International Islamic University Malaysia, Malaysia

⁴Department of Manufacturing and Materials Engineering, Faculty of Engineering, International Islamic University Malaysia.

⁵Department of Engineering, Lancaster University, Lancaster, LA1 4YW, UK

^aarifrahat@sunway.edu.my, ^bfaris@iium.edu.my, ^czahangir@iium.edu.my, ^dahsanalikhano912@gmail.com, ^esaidur@sunway.edu.my

* For correspondence: A. Arifutzzaman: Email: arifrahat@sunway.edu.my, Contact: +601-82500971 (cell).

Keywords: Nanofluids; Graphene; Maghemite; Thermal conductivity; Flake Geometry; Effective Medium Theories.

Abstract. Reasoning of particular mechanism of anomalous thermal transport behaviours are not identified yet for the nanofluids. In this study, iron oxide (Maghemite: MH) and graphene (Gr) flake dispersed deionized water (DW) hybrid nanofluid system were developed for the first time to evaluate the thermal conductivity (TC) enhancements along with the analysis of anomalous TC behavior implementing modified effective medium theories (EMTs). A solvo-thermal two-step method was used to develop the MH nanoparticle and exfoliated Gr flake dispersed hybrid nanofluids with different compositions. Stability of as-prepared hybrid nanofluids were monitored using Ultraviolet-Visible (UV-Vis) spectroscopy. The maximum sedimentation rate was observed ~ 8.4 % after 600 hours. The results showed an overall maximum TC enhancement of ~ 43 % at 25 °C. EMTs were modified with the consideration of flat geometry of Gr flake. It is found that, modified EMTs with the crumpled factor (due to the non-flatness or crumple of Gr flake) of ~ 0.205 the predicted effective TC enhancements are agreed with the experimental TC's of Gr-NMP/MH-DW hybrid nanofluids samples. The estimated crumple factor value of exfoliated Gr flakes using images analysis was also found nearly similar (~ 0.232). This agreement exposed that, Gr flake's with negligible thickness compared to its extremely wide basal plane dimensions and its non-flatness or crumpled geometry in the nanofluids have the leading impacts on the effective TC properties of the Gr flake dispersed nanofluids. This modified model opens the new doors to analyse the insight of the thermophysical properties of various types of nanofluids by introducing potential other parameters.

1 Introduction

Cooling is one of the most crucial technical issues in verity of high-tech engineering sectors [1, 2]. Nanofluids have been applying to transfer heat from the modern engineering systems [3-7]. Various physical and chemical factors are anticipated to play their corresponding vital roles on the nanofluid's heat transfer behaviors such as volume fraction [8, 9], species of nanoparticles [10], varying temperature [9, 11] as well as size of nanoparticles [12]. Implication of iron oxides such as magnetite (Fe_3O_4) and maghemite ($\gamma\text{-Fe}_2\text{O}_3$) nanoparticles dispersed nanofluids attracted very potential in miniaturized modern technology in numerous engineering applications [2, 3]. Because they possess an unique combination of super-magnetic behaviours and high magnetization, despite they have lower saturation magnetization and specific power loss, non-toxic and stable against oxidation than metallic particles [13]. Maghemite nanoparticles are essentially more chemically stable than the magnetite nanoparticles in nanofluids [2, 6]. However, due to the necessity of large quantities of heat transfer, ironoxide nanofluids are not a very widespread solution to those applications. Incorporation of high thermal conductive material in fluids enhances the TC of hybrid solid-liquid suspensions [3, 7]. Two dimensional Graphene (Gr) with the negligible thickness compared to basal plane lengths [14] is the most comparable nanomaterial because of the exponentially high thermal-electric conductivity, high mechanical strength and high mobility of charge carriers [15, 16]. Estimated thermal boundary resistance of Gr is $\sim 3.5 \times 10^{-9} \text{ m}^2\text{K W}^{-1}$ [14] while this value for CNT is $8.3 \times 10^{-8} \text{ m}^2\text{K W}^{-1}$ [17]. Small loading of Gr in nanofluids can enhance the significant heat transfer due to extremely large surface areas of Gr flakes contributed in the suspension [4, 9]. Most of the hybrid nanofluids are prepared by two-step technique [18, 19]. Where nanoparticles are synthesized with the aid of different chemical or physical approaches separately then added into the specified base fluid with the aid of sonication and stirring or magnetic force agitation [8, 18-20]. Stability hampers the TC properties of the nanofluids [6, 21]. UV-Vis spectrophotometer is the most widely used approach for the estimation of rate or percentage reduction of sedimentation of the nanofluids [5, 22].

Several studies have been carried out on the ironoxide and carbon-based nanoparticles dispersed hybrid nanofluids [2, 6, 7, 9, 18, 20, 23]. In this work, **it has been** developed and investigated the TC enhancements of water-based Gr flake and MH ($\gamma\text{-Fe}_2\text{O}_3$) nanoparticles dispersed new hybrid nanofluids. Water and MH-DW suspension are not able to fulfil the requirement for the higher heat transfer and heat transfer improvement in special conditions. To ensure this issue, the nanofluid with the mixture of Gr flake and MH nanoparticles and water could be a good option. Thus, morphology of the particles, TC and stability have been evaluated to investigate the suitability of this material in different applications.

Although, the exact mechanism of thermal transport phenomenon in nanofluids are not known yet but, there have been several theories explaining the mechanisms behind the anomalous behaviour of nanofluids' TC [20, 24, 25]. Those are considered as Brownian motion of particles [25], micro convection of cells [26], liquid layering [27], ballistic transport of energy carriers [24] and nanoparticle percolation inside the base fluids [28]. Studies discovered that the Gr nanosheets and CNTs conduct current and heat by Ballistic flow of phonons [29-31]. For this reason, Gr nanosheets or CNTs are likely to dominate the enhancements of TC of the Gr or CNT suspended nanofluids. It is considered that in nanofluids ballistic heat is conducted in Gr or CNT and diffusive heat conduction occurs in liquids, which was previously considered that the heat conduction in both solid and liquid occurs through diffusion. Ballistic heat conduction is far greater than the thermal diffusion [24]. The existence of an ordered interfacial layer of liquid molecule on the suspended spherical particles might not be solely liable to increase of TC anomalously. This mechanism could work if the size of the particle is very small such as less than 10 nm [3]. Existing theoretical models provided a limited physical understanding into the experimental observations [28]. No widely accepted model is still available to predict the values and trends for the experimental data. Few

studies have been reported on prediction of TCs of nanofluids using EMTs considering various size, shape of particles [12, 14, 23, 28, 32] and anisotropy of carbon-based materials [3, 11, 24, 33]. However, based on the knowledge no works found on the theoretical explanations emphasizing the non-flatness or crumple geometry of Gr flake on the effective TC of the hybrid nanofluids.

Novelties of the present study are highlighted below:

Development of water-based Gr flake and γ -iron oxide new hybrid nanofluids and evaluation of TC with the effects of Gr content on TC enhancement of this hybrid nanofluid system. Modification of the EMTs by considering the anisotropy of the Gr flake's non-flatness or crumple effect on the TC of nanofluids and achieving their experimental evidence with the morphology analysis are unique phenomena seek to address. Executions of modified EMTs for the prediction of anomalous TC behaviour of the as produced water-based Gr flake and MH nanoparticles dispersed hybrid nanofluids is a new spectacle which is also one of the main distinctiveness of this study. The illumination of the impelling influence of volume fraction of filler and temperature on the stability analysis is also an outstanding finding of this work. New correlations for the TC as a function of nanofluids temperature and dispersed fillers amount are developed using experimentally acquired data.

2 Experimental and Theoretical

2.1 Preparation of Maghemite-Gr Hybrid Nanofluids. Maghemite (MH)-Gr hybrid nanofluids were prepared by a solvothermal two steps approach [18]. Firstly, synthesized MH nanoparticles from chemical co-precipitation technique were taken and peptized in DW. It was then stirred for about 2 hours using a magnetic stirrer with 200 rpm to break any agglomerations. Then this suspension was filtered by membrane filter ($\leq 0.22 \mu\text{m}$) using a vacuum filtration unit. Filtered MH dispersion in DW (MH-DW) was collected in the filtration beaker. A homogeneous dispersion was obtained. Secondly, Gr flakes were synthesized by liquid phase exfoliation (LPE) technique in an organic solvent NMP. Exfoliated Gr in NMP solvent is expressed as Gr-NMP in this study. Processing and characterization of Gr-NMP are explained elsewhere in Arifutzzaman et al., (2018 and 2019) [34, 35]. To prepare the hybrid nanofluid samples, exfoliated Gr-NMP flakes were added as filler into the MH-DW base fluid. The hybrid mixture was bath sonicated in BRANSONIC (Model. 3510E-MTH, 100 W, 42 KHz) ultrasonic cleaner for 15 min. Then stirred for one hour using the magnetic stirrer. A uniform and homogeneous dispersion was obtained.

The effect of the addition of Gr filler on TC of the MH-DW nanofluid was investigated. Five hybrid nanofluid samples with five different compositions were prepared. In the hybrid samples Gr content varied in the MH-DW suspension. In the hybrid fluid, MH-DW was considered as the base fluid and the added Gr acted as filler. Concentration ratios of MH and Gr in the hybrid samples were 1:0.3, 1:0.45, 1:0.6, 1:0.75 and 1:0.9 respectively. For the explanation purpose, the hybrid nanofluid is represented as Gr-NMP/MH-DW. The sample corresponds as short form 'S'. So, hybrid samples are expressed as S1: Gr-NMP/MH-DW, S2: Gr-NMP/MH-DW, S3: Gr-NMP/MH-DW, S4: Gr-NMP/MH-DW and S5: Gr-NMP/MH-DW for the compositions of 1:0.3, 1:0.45, 1:0.60, 1:0.75 and 1:0.9 respectively.

2.2 Morphology Analysis. The morphology of the sonication assisted exfoliated Gr flakes was inspected by field emission scanning electron microscopy (FESEM) (Model JEOL JSM-6700F). Few drops of suspension were dripped onto the copper stub and dried by air flow. A gold coat was made on the samples using sputter coating technique before taking the images to avoid the charging during the capturing the images. Image analysis software OLYMPUS Stream (version 1.9) was used for the analysis of collected images.

2.3 Thermal Conductivity Measurements. TC of Gr-NMP/MH-DW hybrid nanofluid samples was measured by the KD2 Pro device (Decagon, USA, version 5) using KS-1 single-probe sensor. An up-to-date programmable refrigerated water bath (Model AD07R-40-12E, Polyscience, USA)

was used for governing the temperature which can preserve temperature uniformity within ± 0.01 °C. Sensor performance was measured with manufacturer recommended fluid glycerol. About 45 ml of Gr-NMP/MH-DW hybrid nanofluid sample was taken into a close vial. A thermocouple was placed inside the vial to monitor the inside sample temperature. Sensor probe was wholly inserted vertically into the sample vial. The schematic explanation of the TC arrangement is shown in Fig. 1(a). Experimental setup details in the laboratory is shown in Fig. 1(b). Deviation of the noted temperature was ± 0.5 °C. All measurements were conducted within the same range of temperature 25 to 60 °C. Data was noted for every temperature only after reaching the equilibrium state. For the accuracy purpose, every data was taken repeatedly minimum of 10 times (up to 25 times). Absolute errors of all measurements were found ± 0.001 . It means that experimental values of TC's were well fit with the equation used in the KD2 pro equipment [36]. Almost 20 % of collected data were not taken for analysis pretending them as outliers. Average values were taken for the analysis. After the above stated cautious measures in procedures and data collection, it gains strong confidence on the experimental results.

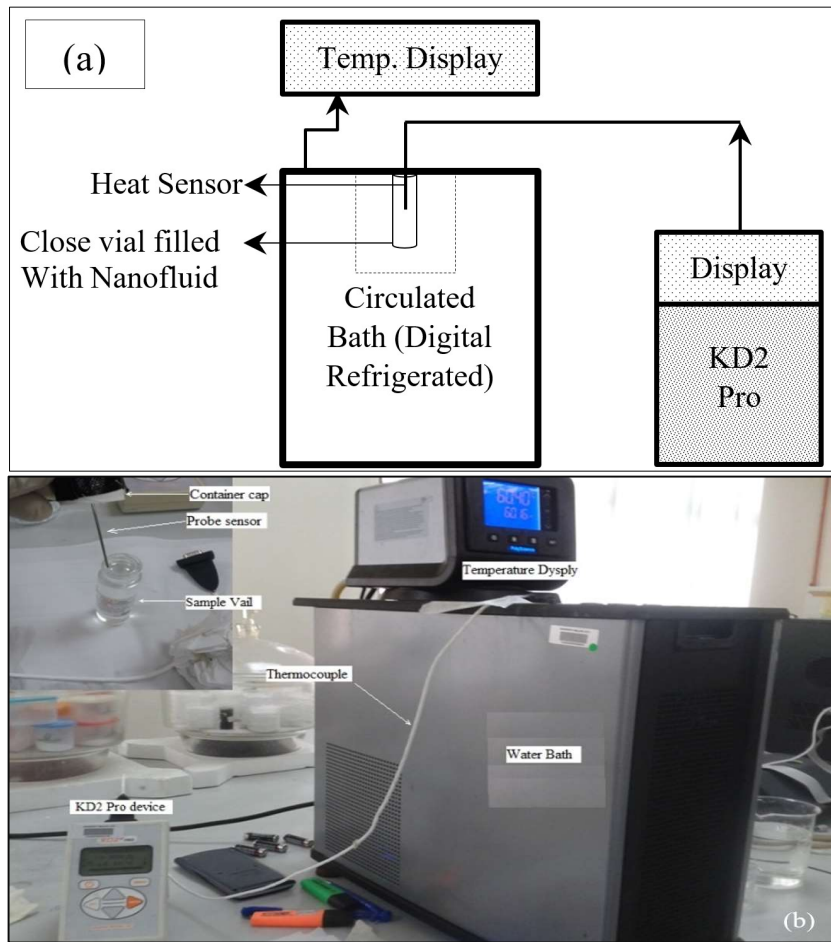


Fig. 1. Thermal conductivity measurement instrument: (a) Schematic illustration, (b) Experimental setup details.

2.4 Stability Monitoring of Gr-NMP/MH-DW Nanofluids. Digital photographs were captured for the visual observations of the physical appearances of Gr-NMP/MH-DW hybrid nanofluid samples. A systematic stability analysis of the Gr-NMP/MH-DW hybrid samples were conducted at room temperature by measuring the optical absorbance using UV-Vis spectrometer (Thermo

Scientific, Multiskan GO, Version-1.00.40. 96-grid transparent micro-plates). First, after preparation every samples were scanned for three times using UV-Vis spectrometer within the light wavelength from 200 to 800 nm. Peak absorbance was detected for every sample to a certain wavelength. Then, the standard graph was plotted for sample concentrations (C_o) against their corresponding peak absorbance'. The concentration of the suspensions has a linear relationship with absorbance. At the last step, the relative concentrations of the prepared hybrid nanofluids were examined with the increasing time. Through that, UV-Vis spectrometer scanning was accompanied on the supernatant of each sample in about 120 hours' interval for 25 days. Supernatant concentration (C) of the hybrid sample was evaluated for the equivalent absorbance. The relative concentrations (C/C_o) of the samples were fit against time.

2.5 Effective Medium Theories (EMTs)

For the prediction of TC of solid-liquid suspensions rule of mixture (ROM) theory has been implemented by Nielsen, (1973) [37]. ROM theory is expressed as Eq. (1),

$$K_{eff} = K_f + \frac{\varphi(K_p - K_f)}{(K_p - \varphi(K_p - K_f))} \quad (1)$$

Maxwell [38] model in Eq. (2) is the representative of conventional analytical models developed considering very diluted suspension of the spherical shaped particles and without counting the interactions among particles. Where, K_{eff} is the effective TC of the suspension, K_p is the TC of the solid particles, K_f is the TC of the base fluids and φ is the volumetric fraction of the suspended filler.

$$K_{eff} = \frac{(K_p + 2K_f) + 2\varphi(K_p - K_f)}{(K_p + 2K_f) - \varphi(K_p - K_f)} \times K_f \quad (2)$$

Common Maxwell Gantt type Effective Medium Approximation (MG-EMA) in Eq. (3) was rediscovered by considering interfacial thermal resistance for the several ellipsoidal particle geometries, topologies and orientations in the matrix [39-42].

$$K_{eff} = K_f \frac{2 + \varphi_p[\beta_{11}(1 - L_{11})(1 + \langle \cos^2 \theta \rangle) + \beta_{33}(1 - L_{33})(1 - \langle \cos^2 \theta \rangle)]}{2 - \varphi_p[\beta_{11}L_{11}(1 + \langle \cos^2 \theta \rangle) + \beta_{33}L_{33}(1 - \langle \cos^2 \theta \rangle)]} \quad (3)$$

Where L_{ii} is the well-recognized geometrical factor based on the principal axes of non-spherical (spheroid) particles dependent on the shape of the particle [32, 43]. L_{ii} is expressed as the function of aspect ratio (∂) of non-spherical filler. Aspect ratio, $\partial < 1$ is for an oblate spheroid where $a_3 < a_1 = a_2$ [14, 41]. Thus, along the three dimensions of the non-spherical it related as, $L_{11} = L_{22}$ and $L_{33} = 1 - L_{11}$. Aspect ratio, $\partial < 1$ is for an oblate spheroid where $a_3 < a_1 = a_2$, on the other hand, $\partial > 1$ is for a prolate spheroid where $a_3 > a_1 = a_2$ [14, 41].

On the other hand, β_{ii} is the function of TC ($K_p - K_f / K_f + L_{ii}(K_p - K_f)$) [33, 41, 42] and the term, $\langle \cos^2 \theta \rangle$ is introduced as the average orientation factor ($\int \rho(\theta) \cos^2 \theta \sin \theta d\theta / \int \rho(\theta) \sin \theta d\theta$) [41, 44]. Where, θ is the angle between the materials

axis and the local particle symmetric axis, (θ) is a distribution function relating to the orientation of the ellipsoidal particle.

2.5.1 Modification of EMTs for Flat Particle Geometry. It was considered that suspended particles are randomly oriented in the based fluid. Thus, the average orientation factor $\langle \text{Cos}^2\theta \rangle = 1/3$ [33]. Therefore, Eq. (3) could be confined as Eq. (4). It is anticipated as general MG-EMA origination for the TC enhancement of the arbitrary isotropic particulate dispersion. It comprises the effects of the aspect ratio, diameter and volume fraction of the filler as well as interfacial thermal resistance and TC ratio of K_p/K_f on the effective TC of the suspension.

$$K_{eff} = K_f \frac{3 + \varphi_p [2\beta_{11}(1 - L_{11}) + \beta_{33}(1 - L_{33})]}{3 - \varphi_p [2\beta_{11}L_{11} + \beta_{33}L_{33}]} \quad (4)$$

Fig. 2 shows the schematic illustration of the dimensions associated with the spheroid (oblate and prolate) filler geometry.

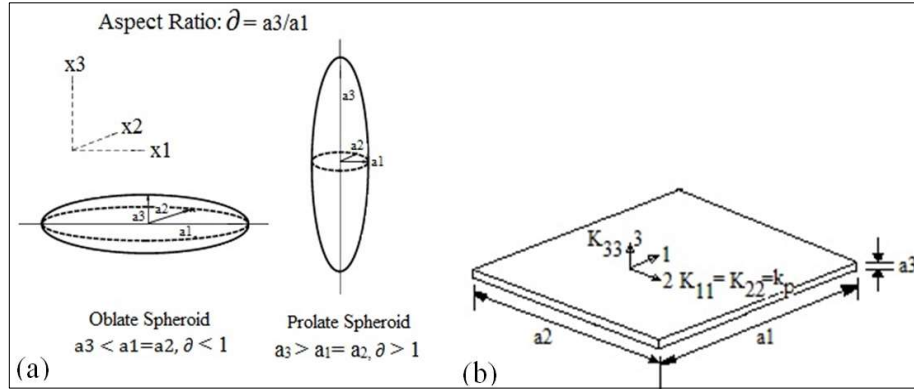


Fig. 2. Schematic illustration (a) dimensions of oblate and prolate spheroid, (b) composite unit cell of a Gr flat plate indicating that $a_1=a_2 \gg a_3$. The equivalent TC along the basal plane of the plate is $K_{11} (= K_{22}) = K_p$ and TC normal to the basal plane is K_{33} .

An ideal Gr flake can be assumed as an oblate spheroid with the aspect ratio of $\vartheta = a_3/a_1 \rightarrow 0$ [14], (as $a_1=a_2 \gg a_3$) which means, the Gr flake possesses ultra large basal plane dimensions ($a_1=a_2$) comparing to negligible thickness normal to the basal plane direction (a_3). Considering this negligible aspect ratio, Gr flake can be treated as a flat plat as in Fig. 2(b). For flat plate, the geometrical factors, $L_{11} = 0$ then $L_{33} = 1$ [41]. So, the β_{ii} function would be modified as $\beta_{11} = K_p/K_f - 1$ and $\beta_{33} = 1 - K_p/K_f$. Thus, the Eq. (4) is modified as Eq. (5) for the TC enhancement of Gr flake suspended nanofluids. Essentially, only one isotropic TC, K_p was observed for in the Gr flakes. This simple relation exhibits an enormous TC enhancement due to influence of large TC of the Gr flakes [45].

$$\frac{K_{eff}}{K_f} = 1 + \frac{2}{3} \varphi \frac{K_p}{K_f} \quad (5)$$

If Gr flakes are incorporated with interfacial thermal resistance, R_{bd} then equivalent TC through flake basal plane is, $K_p^{bd} (K_p / (1 + 2R_{bd}K_p / L)K_p)$ [27, 33, 40]. Here, L is the contributed or equivalent length (L_p^e) of the flake in the suspension. Thus, the effective TC enhancement would be modified as Eq. (6),

$$\frac{K_{eff}}{K_f} = 1 + \frac{2}{3} \varphi \frac{1}{K_f} \left[\frac{K_p}{1 + \frac{2R_{bd}K_p}{L}} \right] \quad (6)$$

It is well identified that the graphite is highly anisotropic in thermal conduction. In the basal plane of graphite TC is estimated within range of 940 to 2000 W/mK, in contrast TC along the normal to the basal plane can vary only between 5 and 20 W/mK [46]. Since few layered Gr flake is the exfoliated peeled off curled graphite structure [47, 48]. For this reason, it is well expected that, Gr flake's TCs through basal plane also would be larger than that of normal ones. Above observation leads to generate the idea to analysis systematically the experimental data with the effect of anisotropy and not-flatness or non-straightness of Gr flake on the effective TC of the Gr flake dispersion using MG-EMA.

Microscopic observations show that, low loaded uniformly dispersed Gr flakes in base fluid are being far apart from straight or completely flat where basal plane of Gr flake is prevailed as crumpled or non-flat sheets in the dispersion. Because, ultrathin Gr flak able to possess enormously large surface. While its thickness is negligible compare to the straight path in basal plane dimensions of that large surface. A schematic illustration of crumpled or non-flat Gr flake is presented in Fig. 3.

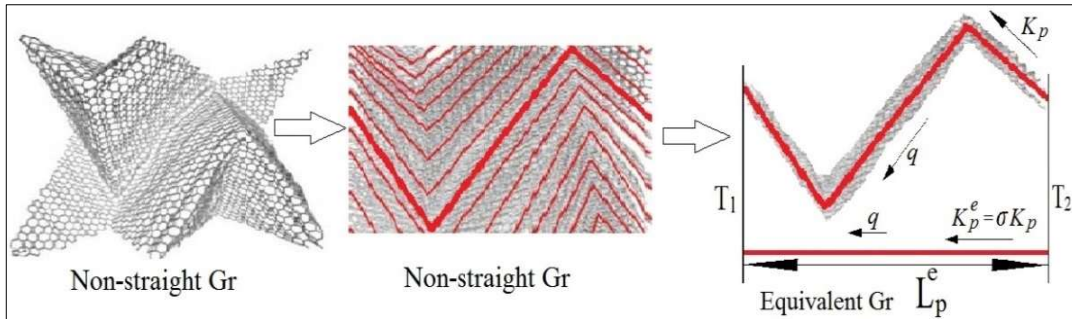


Fig. 3. Schematic illustrations of the crumpled/ non-flat and equivalent Gr flake.

Gr flakes are highly anisotropy in terms of thermal conduction [45]. It means for Gr flake $K_{11} = K_{22} = K_p \gg K_{33}$ thus, $K_{11}/K_{33} = K_p/K_{33} \gg 1$ (Fig. 2b). For this reason, Gr flakes induce a unique property that individual Gr flake is perfect for thermal conduction path through basal plane with negligible flux loss during the long-distance thermal conduction. For non-straight or crumpled Gr flake with non-straight length L_p under a two-end temperature difference $\Delta T = T_2 - T_1$ as shown in Fig. 3. The thermal flux $q = K_p \Delta T / L_p$ is the thermal transport through basal plane of flat Gr flake. It can regard that, this Gr flake as equivalent straight thermal flake such that the equal thermal flux q is conducted (Fig. 3) in between the two ends of the Gr flake in the equivalent straight distance (L or L_p^e). For this reason, the equivalent straight thermal length can relate with flatness or

crumpled ratio of usual length, $\sigma = L_p^e / L_p$. Consequently, the TC through the equivalent straight length is, $\sigma = K_p^e / K_p$. Hence, effective TC of the suspension with the crumpled factor is reformed as Eq. (7).

$$\frac{K_{eff}}{K_f} = 1 + \frac{2}{3} \sigma^2 \phi \frac{K_p}{K_f} \quad (7)$$

3 Results and Discussion

3.1 Morphology Analysis. Fig. 4(a) shows FESEM images of the illustrative folded Gr flakes which fell over on one edge with small isolated fragments of exfoliated Gr on its surface. Fig. 4(b) shows the representative Gr flake that appears crumpled for the exfoliated Gr samples by solvents NMP. Low loaded uniformly dispersed Gr flakes in base fluid are being far apart from straight or completely flat where basal plane of Gr flake is prevailed as crumpled or non-flat sheets in the dispersion [49]. Because, ultrathin Gr flak possesses enormously large surface, its thickness is negligible compared to the straight path in basal plane dimensions of that large surface [14].

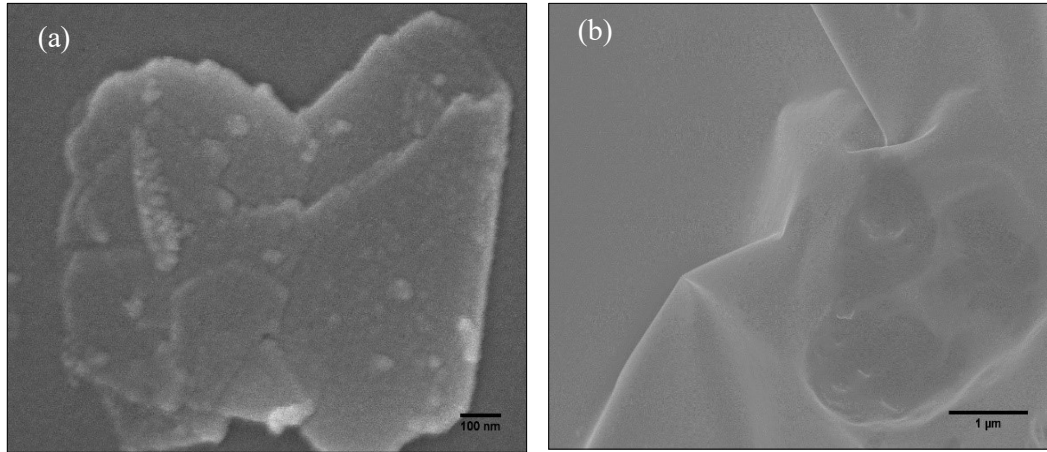


Fig. 4. FESEM images of representative exfoliated Gr flake: (a) folded and (b) crumpled.

3.1.1 Estimations of Crumpling or Non-flatness of Exfoliated Gr Flake. For the analysis of non-flatness of exfoliated Gr flakes, dimensions of around 50 non-flat, crumpled and folded Gr flakes are measured using image analysis software. Sonication assisted exfoliated Gr-NMP was taken as the representative sample. It is seen that, straight or lateral lengths (L or L_p^e) of the Gr flakes measured are varied from ~ 0.481 to $\sim 5.182 \mu\text{m}$. The data are summarized in the histogram shown in Fig. 5(a). Average value of L_{ep} is obtained $\sim 2.771 \mu\text{m}$. Similar procedure have been used to select the size of liquid phase exfoliated Gr flakes by Khan et al., (2012) [48].

On the other hand, the non-straight lengths (L_p) of each flake were also measured (as in Fig. 3). Ratio (σ) of equivalent or lateral and non-straight lengths ($\sigma = L_p^e / L_p$), is obtained by individually dividing the measured value of L_p^e by the value of L_p for each of the Gr flakes measured. Obtained ratios are summarized in the histogram presented in Fig. 5(b). For the flakes this ratios (σ) are the unit less factor and varied from 0 to 1. It is seen that, within the range of 0 to 1 the estimated ratios

(σ) are found varied for ~ 0.071 to ~ 0.681 respectively. From the analysis average value of this ratio (σ) is obtained 0.232.

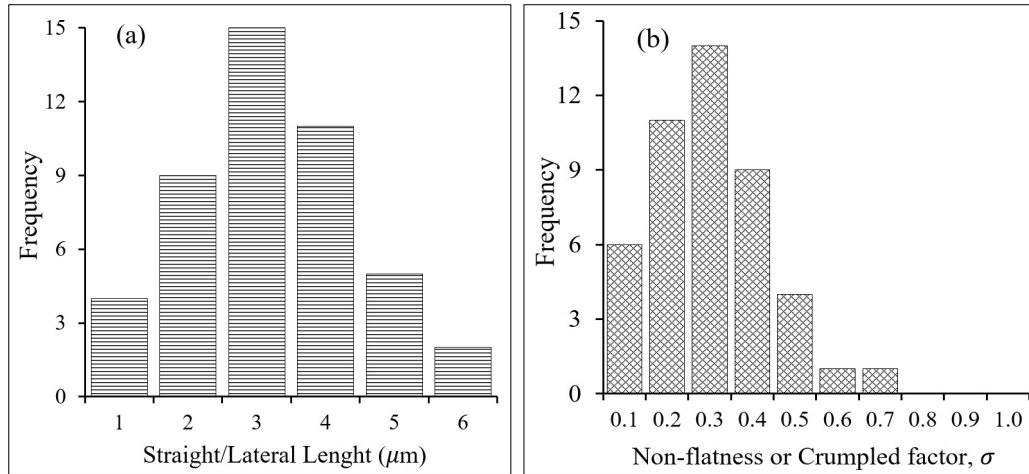


Fig. 5. Histograms (a) flakes straight or lateral or equivalent lengths, (L_p^e) and (b) ratio of Gr-NMP flake's equivalent and non-straight length of the measured Gr-NMP flakes.

FESEM investigation shows the morphology of the produced maghemite ($\gamma\text{-Fe}_2\text{O}_3$) particles by chemical co-precipitation method. *Fig. S1(a)* shows the FESEM micrograph of maghemite ($\gamma\text{-Fe}_2\text{O}_3$) sample. It shows that the particles are mostly spherical in shape.

Fig. S1(b) shows the size distribution of the particles obtained from the FESEM analysis. For the estimation of average size of the synthesized MH nanoparticles, it was conducted the measurements of about 150 particles using image analysis software. It is found that, the sizes of the particles are varied from 7.21 to 80.45 nm among the measured particles. The data are summarized in the histogram in *Fig. S1(b)*. It shows that, particles are uniformly distributed. The average size of the particle is obtained around 23.14 nm. Particle size roughly agrees with the data calculated from the XRD analysis.

Fig. S2 shows the acquired XRD pattern on the synthesized ironoxide particle sample. The diffractogram pattern shows well distinct peaks, this clearly indicates that the ironoxide sample is crystalline in form. No extra salt or ion is detected on XRD analysis. The diffraction peaks at $2\theta = 30.42, 35.60, 43.06, 53.40, 57.25$ and 63.13° are completely matched with the maghemite's ($\gamma\text{-Fe}_2\text{O}_3$) peaks. Square solid dots are placed to indicate the peak positions. The diffraction angles of these peaks are consistent with the standard from maghemite ($\gamma\text{-Fe}_2\text{O}_3$) (JCPDS No. 39-1346) [50]. It shows a reasonable match with previous results reported in the literature [13]. This confirms the formation of maghemite phase of ironoxide. The FWHM of the enlarged peak is used to estimate the average crystallite size with the aid of Scherrer's equation. The average crystallite size of the analyzed sample is found ~ 20.48 nm. The inter-planar spacing of maghemite sample is obtained about 2.51 which is same as the standard value of maghemite (2.51) compared with magnetite's (2.53) [51].

Gr flakes were synthesized by liquid phase exfoliation (LPE) technique in an organic solvent NMP. Processing and characterization of Gr-NMP are explained elsewhere in Arifutzzaman et al., (2018 and 2019) [34, 35]. Exfoliated Gr-NMP were characterized by Raman Spectroscopy. Representative Raman spectrum of the Gr-NMP is shown in *Fig. S3*.

3.2 Stability Investigation of Gr-NMP/MH-DW Hybrid Nanofluids. Fig. 6 shows the physical appearance of the Gr-NMP/MH-DW hybrid nanofluid samples. Digital photographs in Fig. 6(a) and Fig. 6(b) show the hybrid samples of Gr-NMP/MH-DW nanofluids immediately after preparation and 25 days later respectively. Number 1, 2, 3, 4 and 5 tagged on the vials represent the S1, S2, S3, S4 and S5 of Gr-NMP/MH-DW samples respectively. It is apparent that, particles are uniformly dispersed and there is no visible sedimentation in any of the suspensions.

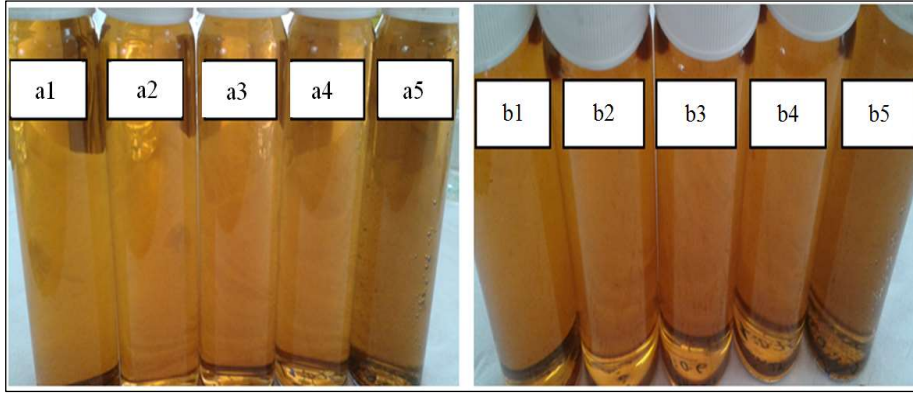


Fig. 6. Digital photographs of the Gr-NMP/MH-DW hybrid nanofluid samples.

3.2.1 UV-vis Spectroscopy. Fig. 7(a) displays the absorbance of Gr-NMP/MH-DW hybrid nanofluids samples with varying wavelengths. The peak absorbance appears at the wavelength of ~ 340 nm. For a Gr-NMP/MH-DW hybrid nanofluid sample the UV-Vis spectrum is featureless with a drastic reduction in absorbance with the increasing wavelength. Moreover, absorbance of the hybrid nanofluid samples reduces with the lessening amount of Gr-NMP in MH-DW; it should be known that the higher amount of Gr-NMP will rise the absorbance that refers to the better nanofluid dispersion. Fig. 7(b) shows the relationships of the obtained absorbance with the respective Gr-NMP/MH-DW hybrid nanofluid samples. There is a good linear relationship perceived with the absorbance and the respective Gr-NMP/MH-DW hybrid nanofluid samples with varying amount of Gr-NMP in MH-DW, which fulfils Beer's Law and specifies that Gr-NMP flakes are dispersed uniformly in the MH-DW base fluid [5].

Addition of Gr-NMP into MH-DW improved the absorbance than that of the individuals. The local peak in the UV-Vis spectra shifts to the longer wavelength (red-shift). As the absorption and wavelength in UV-Vis spectra of hybrid particle suspended nanofluids depend on the all particles included [20]. It is possible in UV-Vis spectrum of various particles dispersion in water. Materials absorption coefficient is mostly liable for this behavior. In addition, other secondary parameters such as dispersion stability, particle size and shape are also importantly influential the absorption behavior [52].

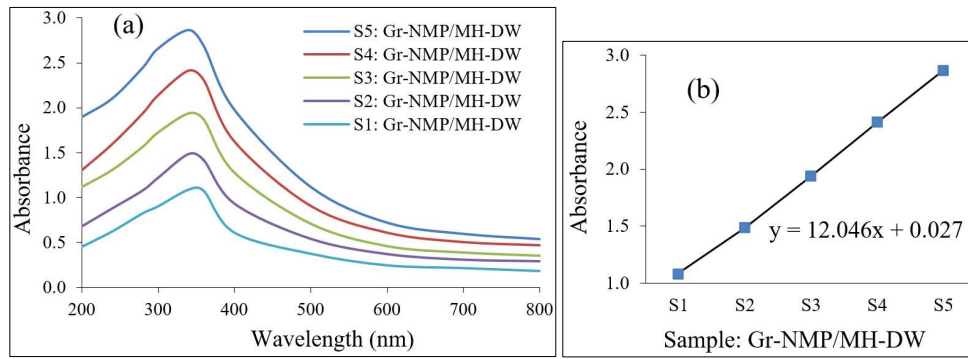


Fig. 7. (a) UV-vis spectrums of Gr-NMP/MH-DW hybrid nanofluid samples with varying amount of Gr-NMP in MH-DW and wavelengths; (b) Linear relationship among the light absorption and hybrid nanofluids samples with varying amount of Gr-NMP in MH-DW for the wavelength of 340 nm.

Absorbance is measured on the on the hybrid nanofluids samples with 120 hours durations. Utilizing the linear relationship in Fig. 7(b), relative concentration (C_0/C) for every hybrid sample of every measurement is estimated and plotted in the Fig. 8. Results show that the relative concentration of the hybrid nanofluids samples are decreased because of the slight agglomeration with the increasing precipitation concentration. Higher Gr-NMP loading causes to more sedimentation. Different forces such as electrostatic force, gravitational force on the particles and van der Waals forces between particles affect in the various nanofluids [5]. It is perceived that, within 120 hours' concentration reduced by only ~ 0.92 , ~ 1.13 , ~ 1.93 , ~ 2.09 and ~ 2.41 % for the samples S1, S2, S3, S4 and S5 of the Gr-NMP/MH-DW hybrid nanofluids respectively. After 25 days, the minimum precipitation rate appears ~ 5.2 % for the hybrid sample S1 and maximum precipitation rate seems to be ~ 8.4 % for the S5 of Gr-NMP/MH-DW. These results show that variation of filler addition affects the rate of precipitation as well as properties, which reach agreement well with the results in previous studies by Mehrali et al., (2014) [5]. It is seen that, the Gr-NMP/MH-DW hybrid nanofluid samples show the lower reduction of relative concentration than the individual which means better stability against the time than that of the individuals. Since, they dispersed uniformly in a polar media DW. Moreover, the density of Gr is smaller than that of MH nanoparticles thus, the gravity's effect on Gr flaks sedimentation is lesser in comparison to that on the MH nanoparticles [20].

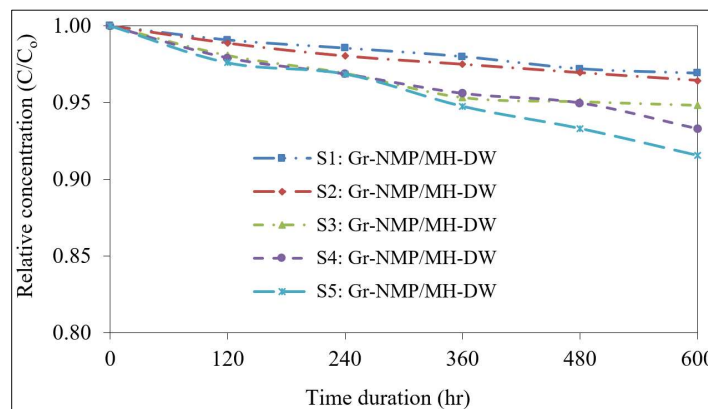


Fig. 8. Relative supernatant concentration of Gr-NMP/MH-DW hybrid nanofluid samples with the increasing sedimentation time.

3.3 TC Enhancements of Gr-NMP/MH-DW Hybrid Nanofluid System

The relative TC of Gr-NMP/MH-DW hybrid nanofluid samples as a function of temperature is shown in the Fig. 9. Relative TC is defined as the ratio of K_{nf} and K_f (K_{nf}/K_f); where, K_{nf} is the experimental TC of the Gr-NMP/MH-DW hybrid nanofluid samples and K_f is the TC of MH-DW as base fluid. It is seen that, relative (K_{nf}/K_f) TC of NMP/MH-DW hybrid samples over MH-DW base fluid is increased linearly from 25 to 50 °C temperature and then it decreased at 60 °C. This phenomenon is also perceived by Das et al., (2003); Han et al., (2008) and Han et al., (2007) [53-55]. Decrease of percentage TC enhancement of every Gr-NMP/MH-DW hybrid samples over the base medium MH-DW at 60 °C due to the contribution of Gr flakes aggregation kinetics [56, 57]. Additionally, Gr sheet suspended (as filler) hybrid nanofluids deteriorate very negligibly by Brownian motion, possibly due to the flexibility of the Gr sheets and ultra-large surface area compared with the negligible thickness [3, 8, 14]. Moreover, due to the increase of temperature Brownian motion of MH particles in the suspension increases, so more mobile particles move rapidly in the base fluid [6]. Thus, judgmentally it could be considered that 50 °C is the critical temperature for the Gr-NMP/MH-DW hybrid nanofluid samples.

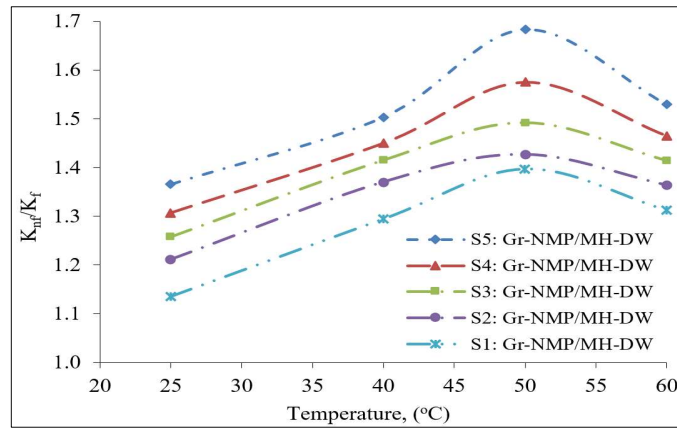


Fig. 9. Relative TC of Gr-NMP/MH-DW hybrid nanofluids over base fluid medium of MH-DW as a function of varying temperature.

3.3.1 Overall Enhancements of TC of Gr-NMP/MH-DW Hybrid Nanofluid System. MH nanoparticles dispersion in DW (MH-DW) limits their use in different applications due to their shallow TC enhancement ability, although it is easily producible and could show a good capability of stable suspension in DW. However, the addition of Gr-NMP in MH-DW nanofluids provides drastic enhancement of TC over the MH-DW because of the contribution of high basal plane TC of Gr flake with the increasing loading of Gr flakes and temperature. Fig. 10 shows the overall percentage TC enhancement of the Gr-NMP/MH-DW hybrid nanofluid samples. It regards the enhancements of TC for the combined effect of MH nanoparticles and Gr flakes addition over DW at rising temperature varied from 25 to 60 °C. For the compression and clarity purposes the data of the thermal conductivity enhancements of Gr-NMP/MH-DW hybrid nanofluid samples in four different temperatures are shown in the tabular format in the inset of the Fig. 10. Overall percentage TC enhancement are calculated using the correlation, $\eta = [(K_{nf}-K_f)/K_f] \times 100 \%$. Here, K_{nf} is the TC of Gr-NMP/MH-DW hybrid nanofluids and K_f is the TC of DW. For the sample S1, percentage TC enhancements over DW are obtained about ~ 19, ~ 41, ~ 59 and ~ 74 % at 25, 40, 50 and 60 °C temperatures respectively. At 25 °C, enhancements of TC's are obtained about ~ 27 and ~ 31 % for the Gr-NMP/MH-DW hybrid samples S2 and S3 respectively which are increased to around ~ 62 and ~ 70 % at 50 °C temperature respectively. Similar trends are observed for the samples S4.

Maximum enhancement of TC is attained for the sample S5. For this sample, it is perceived about ~ 103 % at 60 °C temperature.

It reveals that, the combined effect of Gr flake and MH nanoparticle on the TC enhancements can offer a considerably higher TC of the ultimate Gr-NMP/MH-DW hybrid nanofluid system. Where, effect of Gr flake is much prominent than that of the effect of MH nanoparticle on the TC enhancements of DW. Gr flakes are much higher thermally conductive than MH nanoparticles. TC of Gr increases with the increasing temperature, so the contribution of TC also increases. Moreover, smaller Gr flakes (such as $< 1 \mu\text{m}$) could move randomly with the MH nanoparticles with the increasing temperature so that energy transportation inside the DW becomes stronger [26]. In this case, electron can hop from one Gr flake to another in nanofluid [4]. Besides, it is also observed that, the effect of the amount of Gr addition in the hybrid fluids on the TC enhancement over the base fluid is lower than the effect of temperature on the TC enhancements. This phenomenon was also perceived by Gu, et al., (2014) [58].

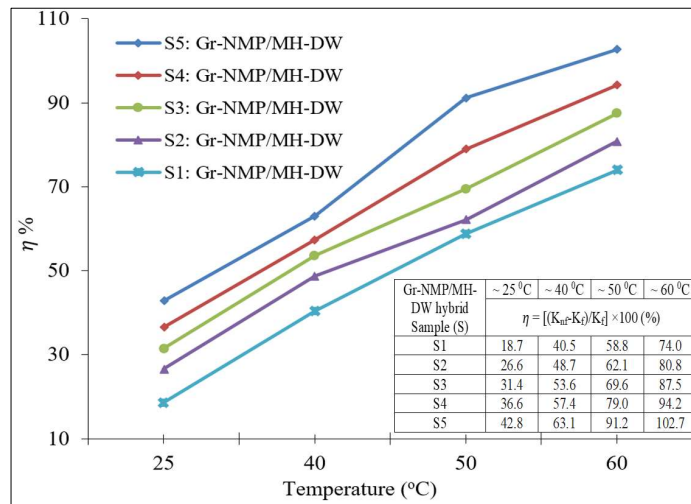


Fig. 10. Overall percentage TC enhancements of the Gr-NMP/MH-DW hybrid nanofluid samples over DW with the varying temperature ranges from 25 to 60 °C. Data in the inset Table are the enhancements in thermal conductivity of the Gr-NMP/MH-DW hybrid nanofluid samples in four different temperatures measured.

3.4 TC Enhancements of Gr-NMP/MH-DW Nanofluids by EMTs

The relative enhancements of experimental TC at 25 °C for Gr-NMP/MH-DW hybrid nanofluid samples are plotted in Fig. 11. The relative TC is defined as K_{nf}/K_f , where, K_{nf} is the TC of the Gr-NMP/MH-DW hybrid nanofluids and K_f is the TC of MH-DW as base fluid. Fig. 11 illustrates the effects of filler Gr-NMP addition on the TC enhancements of Gr-NMP/MH-DW hybrid nanofluid samples over MH-DW base fluid. Estimated TC values of Gr-NMP/MH-DW hybrid nanofluid samples by the Rule of Mixture (ROM) theory (Eq. 1) and Maxwell model (Eq. 2) are also plotted for comparison.

In Fig. 11(a), it is seen that relative TC (K_{nf}/K_f) from both of ROM theory and Maxwell model are shown one (1) for all the Gr-NMP/MH-DW hybrid samples with an increasing amount of Gr-NMP addition in the MH-DW base fluid. It means that, these models predicted effective TC's are almost similar to the hybrid nanofluids base fluid. These predictions are seen to be under predicting awfully from the experimental TC of the hybrid nanofluid samples. It indicates that there are other mechanisms which contribute to the TC enhancement in Gr-NMP/MH-DW hybrid samples.

In both ROM theory and Maxwell model, it is considered that the filler Gr flake is thermally isotropic ($K_{11} = K_{22} = K_{33} = K_p$) with $K_p/K_f \gg 1$. Where, the equivalent TC along the basal plane of the flake is K_{11} and K_{22} and the TC normal to the basal plane is K_{33} (as shown in Fig. 2). In fact, ideal Gr flake is a flat sheet with negligible thickness compared to the flat path dimensions [14]. In this analysis it was noted that at room temperature the TC values of base fluid (MH-DW) is $K_{bf} = 0.631$ W/mK and filler Gr flake TC, $K_p = 3000$ W/mK [59]. Choi, et al., (2001) [24] also found that the theoretical predictions can show only a minor conductivity enhancement for the carbon-based particles suspended nanofluids.

This theoretical model for solid-liquid suspension originated from the Fourier's Law of heat conduction. If it is considered that the thermal diffusion is contributed for the thermal conduction enhancement of carbon-based material suspended nanofluids, then it could be presumed that the theoretical predictions can increase the TC only marginally. For this reason, phenomenal experimental results tend to exhibit essential restrictions in conventional models.

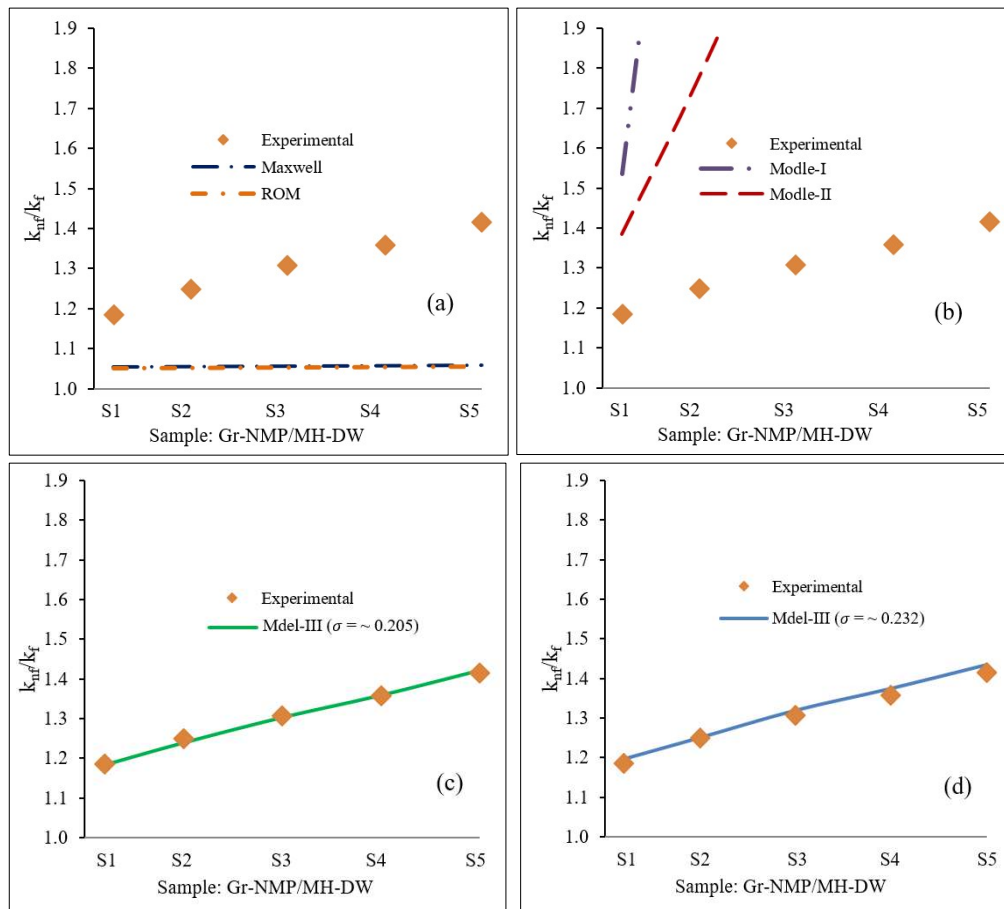


Fig. 11. Experimental (square dots) with models (line graph) TC enhancements of Gr-NMP/MH-DW hybrid nanofluid samples: (a) ROM theory and Maxwell, (b) Model-I and Model-II and (c) Model-III with predicted crumpled factor, (d) Model-III with measured crumpled factor.

Fig. 11(b) also shows the comparison of Model-I and Model-II predictions with experimental TC of Gr-NMP/MH-DW hybrid fluid samples with increasing Gr-NMP amount in the MH-DW base fluid. It is seen that, the modified Model-I predicts very high TC enhancements than that of

experimentally perceived for the Gr-NMP/MH-DW hybrid fluid samples. Model-I is modified by considering the filler Gr flake as a flat plate with their random orientation in base fluid.

Higher prediction of TC by Model-I than the experimental results indicates that there is still an opportunity for the additional enhancements in the TC through the improvement of processing approach and the feature of Gr flakes. The large disagreements between the predictions and present experimental could be because of the interfacial thermal resistance between the base fluid and the Gr flakes.

Effect of interfacial thermal resistance (R_{bd}) on the TC enhancements of Gr-NMP/MH-DW hybrid nanofluid samples is shown using the modified Model-II. In this case, the interfacial resistance, $R_{bd} = 2.89 \times 10^{-9} \text{ m}^2 \text{KW}^{-1}$ is used for the estimation of effective TC of Gr-NMP/MH-DW hybrid nanofluid samples in Model-II. It is seen that the predicted TC enhancements are also highly over predicted than the experimental values. Thus, it also exposes here that, there is a negligible interfacial resistance between the interface of the Gr flake and the base fluid. So, it could be said that, a minor effect of interfacial resistance is witnessed on the effective TC of the Gr-NMP/MH-DW hybrid nanofluids samples. These predictions show that the TC of the Gr-NMP/MH-DW hybrid nanofluid samples are anomalously larger than the conventional theoretical predictions (as explain in Fig. 11(a)), because those models might not be valid for the Gr flake dispersed suspensions.

Model-III prediction with experimental TC enhancements of Gr-NMP/MH-DW hybrid nanofluid samples are plotted in Fig. 11(c). The results expose that the prediction of effective TC by the modified Model-III with non-straightness or crumpled factor (σ) of ~ 0.205 agree well with the measured TC enhancements for Gr-NMP/MH-DW hybrid fluid samples.

On the other hand, the image analysis of the same Gr flakes also gives a nearly similar range of σ value (as shown in Fig. 6). For this value of σ , the predicted TC enhancements by Model-III are also showing a reasonable agreement (as shown in Fig. 11(d)) with the measured TC enhancement of the same Gr flake dispersed hybrid nanofluid samples. It reveals that TC enhancements of Gr nanofluids could be influenced by the contributed lengths and the accordingly contributed TC in the suspension.

4 Conclusions

MH nanoparticle and exfoliated Gr-NMP dispersed hybrid nanofluid system (Gr-NMP/MH-DW) with different compositions were successfully developed by a solvo thermal two steps approach. The lowest and maximum precipitation rates were noted ~ 5.2 and ~ 8.4 % after 600 hours for the hybrid samples S1 and S5 respectively. The effect of amount of Gr addition in the hybrid nanofluid is lower than the effect of temperature on the TC enhancements over the base fluid. Judgmentally, 50°C was found as critical temperature for the Gr-NMP/MH-DW hybrid nanofluid samples in terms of percentage of TC enhancements over MH-DW base fluid. Overall, significantly a high enhancement of TC for the Gr-NMP/MH-DW hybrid nanofluids was attained over the DW. A maximum enhancement of TC was attained 43 % at 25°C and at 60°C temperature it was obtained almost 103 % for sample S5 of Gr-NMP/MH-DW hybrid nanofluid. Prediction of effective TC enhancements of produced nanofluid samples by the rule of mixture (ROM) theory, Maxwell model showed under prediction from the experimental TC's of Gr-NMP/MH-DW hybrid nanofluids. Execution of modified MG-EMA type models revealed that, there is no interfacial thermal resistance active with the Gr flake and fluid interface. It is seen that, for the crumpled factor (due to the non-flatness or crumple of Gr flake) of approximately ~ 0.205 the predicted effective TC enhancements were fairly agreed the experimental TC's of Gr-NMP/MH-DW hybrid nanofluids samples. The estimated value of the crumple factor of exfoliated Gr flakes using images analysis was also found nearly similar (~ 0.232). This agreement exposed that, Gr flake's negligible thickness compared to its extremely wide basal plane dimensions and its non-flatness or crumpled

geometry in the nanofluid have the leading impacts on the effective TC properties of the Gr flake dispersed nanofluids.

5 Supplementary Information (SI)

A supporting Information (SI) file consisting of (i) Title page, (ii) Table of Contents in SI and (iii) Figs, Tables with the captions. APENDICE A in the SI file consists of Morphology and XRD analysis of maghemite (MH) and Raman spectra of the Gr-NMP. APENDICE B consists of *Table SI* as nomenclature of abbreviations, symbols and subscripts used throughout the manuscript.

6 Acknowledgement

The authors courteously acknowledge for allowing the lab facilities under Manufacturing and Materials Engineering Department in International Islamic University Malaysia.

7 References

- [1] S. Khatai, R. Kumar, A.K. Sahoo, A. Panda, D. Das, Metal-oxide based nanofluid application in turning and grinding processes: A comprehensive review, *Materials Today: Proceedings*, (2020).
- [2] P. Agnihotri, V. Lad, Magnetic nanofluid: synthesis and characterization, *Chemical Papers*, (2020) 1-12.
- [3] Z. Han, *Nanofluids with enhanced thermal transport properties*, 2008.
- [4] T.T. Baby, S. Ramaprabhu, Investigation of thermal and electrical conductivity of graphene based nanofluids, *Journal of Applied Physics*, 108 (2010) 124308.
- [5] M. Mehrali, E. Sadeghinezhad, S.T. Latibari, S.N. Kazi, M. Mehrali, M.N.B.M. Zubir, H.S.C. Metselaar, Investigation of thermal conductivity and rheological properties of nanofluids containing graphene nanoplatelets, *Nanoscale research letters*, 9 (2014) 15.
- [6] I. Nurdin, I.I. Yaacob, M.R. Johan, Enhancement of thermal conductivity and kinematic viscosity in magnetically controllable maghemite (γ -Fe₂O₃) nanofluids, *Experimental Thermal and Fluid Science*, 77 (2016) 265-271.
- [7] M.H. Esfe, M.K. Amiri, A. Alirezaie, Thermal conductivity of a hybrid nanofluid, *Journal of Thermal Analysis and Calorimetry*, 134 (2018) 1113-1122.
- [8] H. Xie, W. Yu, Y. Li, L. Chen, Discussion on the thermal conductivity enhancement of nanofluids, *Nanoscale research letters*, 6 (2011) 124.
- [9] L. Yang, W. Ji, Z. Zhang, X. Jin, Thermal conductivity enhancement of water by adding graphene nano-sheets: consideration of particle loading and temperature effects, *International Communications in Heat and Mass Transfer*, 109 (2019) 104353.
- [10] M. Mehrali, E. Sadeghinezhad, A.R. Akhiani, S.T. Latibari, H.S.C. Metselaar, A.S. Kherbeet, M. Mehrali, Heat transfer and entropy generation analysis of hybrid graphene/Fe₃O₄ ferro-nanofluid flow under the influence of a magnetic field, *Powder technology*, 308 (2017) 149-157.
- [11] P.M. Kumar, J. Kumar, R. Tamilarasan, S. Sendhilnathan, S. Suresh, Review on nanofluids theoretical thermal conductivity models, *Engineering Journal*, 19 (2015) 67-83.
- [12] T. Ambreen, M.-H. Kim, Influence of particle size on the effective thermal conductivity of nanofluids: A critical review, *Applied Energy*, 264 (2020) 114684.
- [13] E. Darezereshki, Synthesis of maghemite (γ -Fe₂O₃) nanoparticles by wet chemical method at room temperature, *Materials Letters*, 64 (2010) 1471-1472.
- [14] K.M. Shahil, A.A. Balandin, Graphene–multilayer graphene nanocomposites as highly efficient thermal interface materials, *Nano letters*, 12 (2012) 861-867.
- [15] W. Yu, H. Xie, D. Bao, Enhanced thermal conductivities of nanofluids containing graphene oxide nanosheets, *Nanotechnology*, 21 (2009) 055705.

- [16] A. Arshad, M. Jabbal, Y. Yan, D. Reay, A review on graphene based nanofluids: preparation, characterization and applications, *Journal of Molecular Liquids*, (2019).
- [17] S.T. Huxtable, D.G. Cahill, S. Shenogin, L. Xue, R. Ozisik, P. Barone, M. Usrey, M.S. Strano, G. Siddons, M. Shim, Interfacial heat flow in carbon nanotube suspensions, *Nature materials*, 2 (2003) 731-734.
- [18] J. Sarkar, P. Ghosh, A. Adil, A review on hybrid nanofluids: recent research, development and applications, *Renewable and Sustainable Energy Reviews*, 43 (2015) 164-177.
- [19] K. Bashirnezhad, M.M. Rashidi, Z. Yang, S. Bazri, W.-M. Yan, A comprehensive review of last experimental studies on thermal conductivity of nanofluids, *Journal of Thermal Analysis and Calorimetry*, 122 (2015) 863-884.
- [20] Y. Liu, W. Jin, Y. Zhao, G. Zhang, W. Zhang, Enhanced catalytic degradation of methylene blue by α -Fe₂O₃/graphene oxide via heterogeneous photo-Fenton reactions, *Applied Catalysis B: Environmental*, 206 (2017) 642-652.
- [21] D.W. Johnson, B.P. Dobson, K.S. Coleman, A manufacturing perspective on graphene dispersions, *Current Opinion in Colloid & Interface Science*, 20 (2015) 367-382.
- [22] A. Ghadimi, R. Saidur, H. Metselaar, A review of nanofluid stability properties and characterization in stationary conditions, *International journal of heat and mass transfer*, 54 (2011) 4051-4068.
- [23] A. Omrani, E. Esmaeilzadeh, M. Jafari, A. Behzadmehr, Effects of multi walled carbon nanotubes shape and size on thermal conductivity and viscosity of nanofluids, *Diamond and Related Materials*, 93 (2019) 96-104.
- [24] S. Choi, Z. Zhang, W. Yu, F. Lockwood, E. Grulke, Anomalous thermal conductivity enhancement in nanotube suspensions, *Applied physics letters*, 79 (2001) 2252-2254.
- [25] C. Kleinstreuer, Y. Feng, Experimental and theoretical studies of nanofluid thermal conductivity enhancement: a review, *Nanoscale research letters*, 6 (2011) 229.
- [26] S. Sen Gupta, V. Manoj Siva, S. Krishnan, T. Sreepasad, P.K. Singh, T. Pradeep, S.K. Das, Thermal conductivity enhancement of nanofluids containing graphene nanosheets, *Journal of Applied Physics*, 110 (2011) 084302.
- [27] M. Bryning, D. Milkie, M. Islam, J. Kikkawa, A. Yodh, Thermal conductivity and interfacial resistance in single-wall carbon nanotube epoxy composites, *Applied Physics Letters*, 87 (2005) 161909.
- [28] N.V. Sastry, A. Bhunia, T. Sundararajan, S.K. Das, Predicting the effective thermal conductivity of carbon nanotube based nanofluids, *Nanotechnology*, 19 (2008) 055704.
- [29] J. Hone, M. Whitney, C. Piskoti, A. Zettl, Thermal conductivity of single-walled carbon nanotubes, *Physical Review B*, 59 (1999) R2514.
- [30] E. Munoz, J. Lu, B.I. Yakobson, Ballistic thermal conductance of graphene ribbons, *Nano letters*, 10 (2010) 1652-1656.
- [31] A.V. Savin, Y.S. Kivshar, B. Hu, Suppression of thermal conductivity in graphene nanoribbons with rough edges, *Physical Review B*, 82 (2010) 195422.
- [32] C.W. Nan, Effective-medium theory of piezoelectric composites, *Journal of applied physics*, 76 (1994) 1155-1163.
- [33] F. Deng, Q.-S. Zheng, L.-F. Wang, C.-W. Nan, Effects of anisotropy, aspect ratio, and nonstraightness of carbon nanotubes on thermal conductivity of carbon nanotube composites, *Applied Physics Letters*, 90 (2007) 021914.
- [34] A. Arifuzzaman, A. Ismail, A. Khan, M. Alam, I. Yaacob, Effect of Exfoliated Graphene Defects on Thermal Conductivity of Water Based Graphene Nanofluids, *International Journal of Applied Engineering Research*, 13 (2018) 4871-4877.
- [35] A. Arifuzzaman, A. Ismail, I. Yaacob, M. Alam, A. Khan, Experimental investigation of concentration yields of liquid phase exfoliated graphene in organic solvent media, *IOP Conference Series: Materials Science and Engineering*, IOP Publishing, 2019, pp. 012001.

- [36] D. Decagon, KD2 Pro Theory. , KD2 Pro User Manual, (2006).
- [37] L.E. Nielsen, Thermal conductivity of particulate-filled polymers, *Journal of applied polymer science*, 17 (1973) 3819-3820.
- [38] J.C. Maxwell, *A treatise on electricity and magnetism*, Clarendon press 1881.
- [39] T. Chen, G.J. Weng, W.-C. Liu, Effect of Kapitza contact and consideration of tube-end transport on the effective conductivity in nanotube-based composites, *Journal of applied physics*, 97 (2005) 104312.
- [40] C.-W. Nan, G. Liu, Y. Lin, M. Li, Interface effect on thermal conductivity of carbon nanotube composites, *Applied Physics Letters*, 85 (2004) 3549-3551.
- [41] C.-W. Nan, R. Birringer, D.R. Clarke, H. Gleiter, Effective thermal conductivity of particulate composites with interfacial thermal resistance, *Journal of Applied Physics*, 81 (1997) 6692-6699.
- [42] C.-W. Nan, Z. Shi, Y. Lin, A simple model for thermal conductivity of carbon nanotube-based composites, *Chemical Physics Letters*, 375 (2003) 666-669.
- [43] C.-W. Nan, *Physics of inhomogeneous inorganic materials*, *Progress in materials science*, 37 (1993) 1-116.
- [44] C.W. Nan, X.P. Li, R. Birringer, Inverse problem for composites with imperfect interface: determination of interfacial thermal resistance, thermal conductivity of constituents, and microstructural parameters, *Journal of the American Ceramic Society*, 83 (2000) 848-854.
- [45] W. Yu, H. Xie, W. Chen, Experimental investigation on thermal conductivity of nanofluids containing graphene oxide nanosheets, *Journal of Applied Physics*, 107 (2010) 094317.
- [46] R.W. Cahn, Book Review: *Physics of graphite*. BT Kelly (Applied Science Publishers, London, 1981) pp. 477. price:£ 48, *Journal of Nuclear Materials*, 114 (1983) 116-116.
- [47] Y. Hernandez, V. Nicolosi, M. Lotya, F.M. Blighe, Z. Sun, S. De, I. McGovern, B. Holland, M. Byrne, Y.K. Gun'Ko, High-yield production of graphene by liquid-phase exfoliation of graphite, *Nature nanotechnology*, 3 (2008) 563.
- [48] U. Khan, A. O'Neill, H. Porwal, P. May, K. Nawaz, J.N. Coleman, Size selection of dispersed, exfoliated graphene flakes by controlled centrifugation, *Carbon*, 50 (2012) 470-475.
- [49] C. Cheng, D. Li, Solvated graphenes: an emerging class of functional soft materials, *Advanced Materials*, 25 (2013) 13-30.
- [50] M. Nazari, N. Ghasemi, H. Maddah, M.M. Motlagh, Synthesis and characterization of maghemite nanopowders by chemical precipitation method, *Journal of Nanostructure in Chemistry*, 4 (2014) 99.
- [51] M. Tajabadi, M. Khosroshahi, Effect of alkaline media concentration and modification of temperature on magnetite synthesis method using FeSO₄/NH₄OH, *International Journal of Chemical Engineering and Applications*, 3 (2012) 206.
- [52] S. Jana, A. Salehi-Khojin, W.-H. Zhong, Enhancement of fluid thermal conductivity by the addition of single and hybrid nano-additives, *Thermochimica acta*, 462 (2007) 45-55.
- [53] S.K. Das, N. Putra, P. Thiesen, W. Roetzel, Temperature dependence of thermal conductivity enhancement for nanofluids, *J. Heat Transfer*, 125 (2003) 567-574.
- [54] Z. Han, B. Yang, S. Kim, M. Zachariah, Application of hybrid sphere/carbon nanotube particles in nanofluids, *Nanotechnology*, 18 (2007) 105701.
- [55] Z. Han, F. Cao, B. Yang, Synthesis and thermal characterization of phase-changeable indium/polyalphaolefin nanofluids, *Applied Physics Letters*, 92 (2008) 243104.
- [56] R. Prasher, P.E. Phelan, P. Bhattacharya, Effect of aggregation kinetics on the thermal conductivity of nanoscale colloidal solutions (nanofluid), *Nano letters*, 6 (2006) 1529-1534.
- [57] D. Wen, Y. Ding, Effective thermal conductivity of aqueous suspensions of carbon nanotubes (carbon nanotube nanofluids), *Journal of Thermophysics and Heat Transfer*, 18 (2004) 481-485.
- [58] J. Gu, C. Xie, H. Li, J. Dang, W. Geng, Q. Zhang, Thermal percolation behavior of graphene nanoplatelets/polyphenylene sulfide thermal conductivity composites, *Polymer composites*, 35 (2014) 1087-1092.

[59] A. Arifuzzaman, A. Ismail, I. Yaacob, A. Khan, M. Alam, Experimental investigation and effective medium approximation of thermal conductivity of water based exfoliated graphene nanofluids, *International Journal of Applied Engineering Research*, 13 (2018) 7477-7487.